



HAL
open science

Neutron/gamma pulse shape discrimination in plastic scintillators: Preparation and characterization of various compositions

Pauline Blanc, Matthieu Hamel, Chrystèle Dehé-Pittance, Licinio Rocha,
Robert B. Pansu, Stéphane Normand

► To cite this version:

Pauline Blanc, Matthieu Hamel, Chrystèle Dehé-Pittance, Licinio Rocha, Robert B. Pansu, et al.. Neutron/gamma pulse shape discrimination in plastic scintillators: Preparation and characterization of various compositions. Nuclear Instruments and Methods in Physics Research Section A: Accelerators, Spectrometers, Detectors and Associated Equipment, 2014, 750, pp.1-11. 10.1016/j.nima.2014.02.053 . hal-01082176

HAL Id: hal-01082176

<https://hal.science/hal-01082176>

Submitted on 26 Mar 2020

HAL is a multi-disciplinary open access archive for the deposit and dissemination of scientific research documents, whether they are published or not. The documents may come from teaching and research institutions in France or abroad, or from public or private research centers.

L'archive ouverte pluridisciplinaire **HAL**, est destinée au dépôt et à la diffusion de documents scientifiques de niveau recherche, publiés ou non, émanant des établissements d'enseignement et de recherche français ou étrangers, des laboratoires publics ou privés.

Neutron/gamma pulse shape discrimination in plastic scintillators: preparation and characterization of various compositions

Pauline Blanc,^{1,2} Matthieu Hamel,^{1,*} Chrystèle Dehé-Pittance¹, Licinio Rocha,¹ Robert B. Pansu,² and Stéphane Normand¹

1. CEA, LIST, Laboratoire Capteurs et Architectures Électroniques, F-91191 Gif-sur-Yvette, France
2. Laboratoire de Photophysique et Photochimie Supramoléculaires et Macromoléculaires (CNRS UMR 8531), École Normale Supérieure de Cachan, 61 Avenue du Président Wilson, F-94235 Cachan cedex, France

Abstract

This work deals with the preparation and evaluation of plastic scintillators for neutron/gamma pulse shape discrimination (PSD). We succeeded in developing a plastic scintillator with good neutron/gamma discrimination properties in the range of what is already commercialized. Several combinations of primary and secondary fluorophores were implemented in chemically modified polymers. These scintillators were fully characterized by fluorescence spectroscopy and under neutron irradiation. The materials proved to be stable for up to 5 years without any degradation of PSD properties. They were then classified in terms of their PSD capabilities and light yield. Our best candidate, 28.6 wt% of primary fluorophore with a small amount of secondary fluorophore, shows promising PSD results and is particularly suited to industrial development, because its preparation does not involve the use of expensive or exotic compounds. Furthermore, even at the highest prepared concentration, high stability over time was observed. As a proof of concept, one sample with dimensions 109 mm \varnothing \times 114 mm height (\approx 1 L) was prepared.

Keywords

plastic scintillator; pulse shape discrimination (PSD); neutron detection; fluorescence; scintillation

1. Introduction

From the very beginning of neutron detection, pulse shape discrimination (PSD) between neutrons and gamma rays in plastic scintillators remained one of the holy grails of modern physics, as they were widely considered to be indistinguishable. However, in 1960, F. D. Brooks discovered that doping a standard plastic scintillator (*e.g.*, polystyrene + *p*-terphenyl + POPOP) with a so-called “secondary solvent” (herein 4-isopropylbiphenyl) allowed discrimination of fast neutrons from gamma [1]. His “Plastic 77” was later marketed under the trade name NE-150 but was, unfortunately, discarded after physical alterations appeared a few months after production [2]. Since then, several research groups have tried to address this challenge by various means, leading to different levels of success. Their efforts have involved a chemical approach [3], the use of a given geometry that allows gamma rejection [4], and mathematical approaches using smart algorithms that identify the sharp difference existing between neutron and gamma signals [5]. Recently, Zaitseva and co-workers, presumably inspired by previous work from Brooks, developed a new plastic scintillator composed from highly concentrated 2,5-diphenyloxazole (PPO) and a wavelength shifter (optional), 9,10-diphenylanthracene (DPA), in polyvinyltoluene (PVT) [6a,b]. They showed that good PSD was observed only when a given PPO concentration threshold was reached. This new plastic scintillator is currently being sold, most likely with slight modifications from what was originally described, by Eljen Technologies under

* Corresponding author. Tel: +33 1 69 08 33 25; fax: +33 1 69 08 60 30. *E-mail address*: matthieu.hamel@cea.fr (please do not send commercial e-mails).

the trade name EJ-299-33 [6c-e][7]. In 2012, Feng *et al.* proposed for the first time both spectral and pulse shape discrimination in plastic scintillators, with a triplet harvesting system consisting of an iridium complex [8]. In 2006, a French collaborative effort called Neutromania was initiated for developing new plastic scintillators for this purpose, embedding 5 laboratories from 3 cities and gathering physicists and chemists. This project was the foundation for the work that produced the results presented herein. We will see that a general formulation consisting of {polymer + highly concentrated 1st fluorophore + 2nd fluorophore as wavelength shifter} can be used to prepare various plastic scintillators. The present paper determines their ability, or inability, to discriminate neutrons from gamma. We present herein our results regarding the preparation and characterization of plastic scintillators with various compositions, displaying good neutron/gamma pulse shape discrimination efficiency in the range of existing discrimination methods.

56

2. Experimental

Encapsulated liquid scintillator BC-501A and plastic scintillator BC-408 were obtained from Saint-Gobain Crystals and Detectors (Aubervilliers, France). Plastic scintillator EJ-200 was obtained from Eljen Technologies (supplied by Scionix, Bunnix, The Netherlands). Styrene and vinyltoluene monomers were purchased from Sigma-Aldrich and freshly distilled from CaH₂ prior to use. 1,4-Bis(5-phenyl-2-oxazolyl)benzene (POPOP), 9,10-diphenylanthracene, *p*-vinylbiphenyl, and *p*-terphenyl were also purchased from Sigma-Aldrich. 4-isopropylbiphenyl was purchased from Alfa Aesar. 2,5-Diphenyloxazole (PPO) was purchased from Acros or Sigma-Aldrich. All fluorescent molecules were used as received except *p*-vinylbiphenyl, which was purified by silica gel chromatography. The general procedure for plastic scintillator preparation is as follows. In a flame-dried round bottom flask filled with argon (Ar), the powders were dissolved in the liquids. The gases were then removed using the freeze-pump-thaw technique, and the solution was carefully transferred into a vial for polymerization. After completion, the vial was broken with a mallet and the scintillator was obtained after polishing the raw material. The contours and back were ultimately covered with TiO₂ paint (3 layers, EJ-510 from Eljen Technologies) for better light collection through reflection. The process of preparing these materials has been patented [9].

Pulse shape discrimination was performed by irradiating organic scintillators with an unshielded AmBe ≈ 0.45 GBq, $\approx 30\,000$ n/s source. The radioactive source was located 5 cm away from the scintillator.

Nuclear experiments using the charge comparison method, which allows light component separation, have been performed. Photophysical reasons justifying this method are explained well elsewhere [10].

The experimental set-up is described in Figure 1. A range of plastics and one liquid scintillator are characterized using a Hamamatsu H1949-51 photomultiplier (PMT) for light collection; the anode output is then split three ways. Two of the resulting lines are delayed in time, a key parameter to be tuned, using two NSEC Delay 2058 modules (CANBERRA). The third line is dedicated to triggering a constant fraction discriminator (CFD) 583 (ORTEC) at the incoming signal rate, preceded by a Timing Amplifier 2111 (CANBERRA). The CFD generates a TTL signal, producing a time gate, and its width is also a key parameter requiring optimization. These 3 outputs are plugged into a charge integration device, QDC-VME/CAEN (V465). This device integrates both the total and delayed charges, Q_{Tot} and Q_{Del} , in the time gate.

Light Output (LO) measurements were performed under gamma irradiation using a PMT XP-5500B. Energy spectra are obtained using ²²Na, ⁶⁰Co, ¹³⁷Cs and ²⁴¹Am sources. Their intensities were, respectively, 350 kBq, 130 kBq, 400 kBq, and 380 kBq on 09/17/2013.

Count Rate (CR) measurements were performed under gamma irradiation. Energy spectra were recorded using ²²Na, ⁶⁰Co and ¹³⁷Cs sources, and their intensities were 9.75 MBq on 11/07/11, 240 kBq on 03/14/00, and 206 kBq on 03/14/00, respectively.

94

INSERT FIGURE 1 HERE

96 **3. Results and discussion**

97 *3.1. Preliminary study with liquid scintillator BC-501A*

98 Table 1 summarizes the main characteristics of the studied scintillators. Based on the information
 100 contained in their publications, Brooks' [1] and Zaitseva's [6b] scintillators were reproduced for
 102 overall comparison with our own scintillators. Various forms of Brooks' scintillator were prepared,
 according to the observations and issues stated in the past. Finally, our own scintillators were based on
 an almost identical strategy, integrating the first fluorophore at the highest possible concentration, but
 with a specially designed polymer matrix. Several concentrations in various matrices were studied.
 104 The PSD of a BC-501A liquid scintillator, with excellent n/γ discrimination [11] efficiency, was also
 determined to allow an ultimate reference comparison to be made.

106

INSERT TABLE 1 HERE

108

First, neutron/gamma discrimination efficiency in the liquid scintillator BC-501A was determined.
 110 Both the delayed and total charges were obtained and are referred to as Q_{Del} and Q_{Tot} , respectively. To
 compare those charges as a function of the particle's incident energy deposited in the scintillator,
 112 energy spectra are presented in Figure 2 with ^{137}Cs (206 kBq, 03/14/2000) and ^{22}Na (9.75 MBq,
 11/07/2011) gamma sources. Statistics are sufficient for energy calibration since the Compton Edge
 114 position has been verified to be located at the same position at higher statistics considering
 uncertainties.

116

INSERT FIGURE 2 HERE

118

Compton edges (CE) are fitted with Gaussians and identified for both gamma energy (E_γ) peaks from
 120 ^{22}Na (at 511 keV and 1275 keV) and for the peak from ^{137}Cs (at 662 keV). The Compton edges are
 defined in Equation 1, where ϑ is taken at 180° , when gamma rays are considered backscattered. CEs
 122 are located at 341 keV and 1062 keV for ^{22}Na and at 477 keV for ^{137}Cs , as displayed in Table 2.
 Compton edges are taken at 80% of the decay.

124

$$E_\gamma \times \left[1 - \frac{1}{1 + E_\gamma \times \frac{1 - \cos(\vartheta)}{m_e c^2}} \right] \quad \text{Equation 1}$$

126

INSERT TABLE 2 HERE

128 Those energies used for the further calibration of the comparison of the charges are obtained in terms
 of gamma energy; therefore, the calibration is in keVee, standing for keV electron equivalent. The
 130 neutron gamma discrimination spectrum of BC-501A is presented in Figure 3 where the overlapping
 region of neutrons and gamma rays at low energy is not visible since a low threshold of 1 is applied to
 132 the CFD and induces a cut off in the low energy region. For all energy calibrated spectra presented in
 this paper, electronics are tuned with the same exact parameters, including the low threshold of the

134 CFD, for both gamma and neutron/gamma sources acquisitions. In this paper the ratio of the delayed
to total charge has been corrected by a factor 1000 for practical data plotting considerations.

136

INSERT FIGURE 3 HERE

138

3.2. Optimization of plastic scintillator compositions

140 We then decided to reproduce Brooks' Plastic 77 (made from 10 wt% 4-isopropylbiphenyl, 35 g L⁻¹ *p*-
142 terphenyl, and 0.5 g L⁻¹ 1,4-Bis(5-phenyl-2-oxazolyl)benzene (POPOP) in polystyrene, as described in
Scheme 1) and tried to understand the reasons for its instability in order to achieve a stable
144 composition as shown in Figure 4(a). Indeed, the preparation was rather tedious and scintillators were
often non-usable, as presented in Figure 4(b). Ultimately we discovered that annealing the scintillator
146 at a temperature greater than 200°C in the final stage could chemically stabilize it, and Sample #1 was
obtained by this method.

148

INSERT FIGURE 4 HERE

150

INSERT SCHEME 1 HERE

152 From this experimental procedure, Sample #1 was prepared in 2007 and has not physically changed
since. To further develop this scintillator, increasing the first dye concentration was a priority.
154 Unfortunately, annealing was not efficient for Sample #3 when doped with 15 wt% of 4-
isopropylbiphenyl, and the sample displayed small diffuse white spots after the first week of
156 preparation and became totally white after one month.

158

INSERT FIGURE 5 HERE

160 Based on this observation, we made the assumption that linking the highly concentrated first
fluorophore into the polymer matrix would suppress this whitening effect. Replacing 4-
162 isopropylbiphenyl with the same amount of 4-vinylbiphenyl led to a stable scintillator, Sample #4.

The other method for stabilizing the polymer was to create cross-linking between the polymer chains.
164 Thus, an equivalent of Plastic 77 (namely Sample #5) was prepared by mixing styrene with an
appropriate cross-linking agent. Although we feared the scintillation yield would decrease, we
166 obtained a highly transparent and discriminative scintillator.

If the high concentration of 4-isopropylbiphenyl is responsible for the triplet-triplet annihilation, thus
168 allowing *n*/ γ discrimination, the reason for the presence of *p*-terphenyl inside plastic 77 remained
unclear. Sample #2 was thus prepared with no *p*-terphenyl added and, surprisingly, did not display any
170 PSD.

Neutron gamma discrimination spectra for Samples #1, 2, 4 and 5 are displayed in Figure 6. The 4
172 samples all have dimensions of approximately \varnothing 30 mm \times h 10 mm.

174

INSERT FIGURE 6 HERE

176 To determine a given scintillator efficiency, Figures of Merit (FOM) are calculated when projecting
the bidimensional (2D) discrimination spectrum at a given energy (keVee), as described in Equation 2,

178 where $D_{\gamma-n}$ is the distance separating neutron and gamma peaks at their projected maxima, and both $L_{\gamma-}$
180 $FWHM$ and L_{n-FWHM} are the full widths at half maximum of the gamma and neutron peaks. This FOM
quantifies neutron and gamma peak separation for PSD assessments.

$$182 \quad FOM = \frac{D_{\gamma-n}}{L_{\gamma-FWHM} + L_{n-FWHM}} \quad \text{Equation 2}$$

Standard deviations of FOM, $\sigma(FOM)$, are determined by propagating uncertainties on each parameter.
184 By considering the error on neutron and gamma peak Gaussian fits, and thus their maxima and half
186 maxima positions, we estimate that the error on each term, σ , is ± 1.1 for liquids and 2.1 for plastics
because the peaks are closer and the uncertainties on each peak position larger. Therefore, as described
in Equation 3, the standard deviation on FOM is calculated as follows:

$$188 \quad \sigma(FOM) = \sqrt{\left(\frac{\sigma}{(L_{\gamma-FWHM} + L_{n-FWHM})}\right)^2 \times \left[2 + 4 \times \left(\frac{D_{\gamma-n}}{(L_{\gamma-FWHM} + L_{n-FWHM})}\right)^2\right]} \quad \text{Equation 3}$$

190 The average $\sigma(FOM)$ value is 0.04 for all plastics studied and 0.05 for the BC-501A liquid scintillator.
An example of such projection is given in Figure 7, where a section of the BC-501A 2D spectrum
192 from Figure 3 is displayed at 500 keV $\pm 10\%$.

194 **INSERT FIGURE 7 HERE**

196 Projections at 500 keV from Samples #1, 2, 4 and 5 are also presented in Figure 8.

198 **INSERT FIGURE 8 HERE**

200 As observed in Figures 7 & 8, the BC-501A neutron/gamma separation is significantly greater than
that observed for Samples #1, 2, 4 and 5 and is used as an indicator for very good efficiency.
202 Efficiencies were determined through FOM calculations and are presented in Figure 9 and Table 3 for
energies from 200 to 500 keV.

204 **INSERT FIGURE 9 HERE**

206 **INSERT TABLE 3 HERE**

208 Sample #5 is clearly the best preparation among Brooks' compositions where the polymer matrix has
210 been modified. This sample displays an FOM of 0.93 at 300 keV.

212 3.3. FOM determination of various lab-made plastic scintillators

We then examined the potential to use other primary fluorophores. We finally found an appropriate
214 primary fluorophore highly suitable for scintillation and pulse shape discrimination at a very low cost
per mol. Thus, various scintillators were prepared containing 1 to 29 wt% of this primary fluorophore
216 in the matrix. Scintillators doped with concentrations lower than 10 wt% did not display good n/ γ
discrimination (data not shown), and the first realistic results were obtained at 17 wt%. This plastic

218 scintillator preparation is presented in two different volumes, Sample #6 ($\text{Ø } 48 \text{ mm} \times \text{h } 50 \text{ mm}$) and
220 Sample #7 ($\text{Ø } 75 \text{ mm} \times \text{h } 75 \text{ mm}$), in Figure 10.

INSERT FIGURE 10 HERE

222 Another sample, Sample #8, has been prepared using a higher concentration of the first fluorophore
224 (28 wt%) and a unique dimension of $\text{Ø } 32 \text{ mm} \times \text{h } 27 \text{ mm}$. Sample #8 is presented in Figure 11.

INSERT FIGURE 11 HERE

228 Projections of the neutron/gamma discrimination spectra of Samples #6 and 7 at 400 keVee are
230 presented in Figure 12, while those of Sample #8 are shown in Figure 13.

INSERT FIGURE 12 HERE

INSERT FIGURE 13 HERE

234 In Figure 14 and Table 4, FOMs that have been calculated are presented for energies between 200 and
236 900 keVee.

INSERT FIGURE 14 HERE

INSERT TABLE 4 HERE

240 For industrial purposes, it is extremely important to retain the PSD properties while increasing the
242 volume of the scintillator. As one can see, the PSD is only slightly affected; it is reduced by only \approx
244 30% at all energies. In Sample #7, $\text{Ø } 75 \text{ mm} \times \text{h } 75 \text{ mm}$, neutron/gamma discrimination remains
246 efficient, even at low energy, with an FOM of 0.56 at 300 keVee, despite the PMT diameter not being
248 optimized (50 mm) for such measurements. Sample #6, equivalent in composition to Sample #7 but
250 smaller, $\text{Ø } 48 \text{ mm} \times \text{h } 50 \text{ mm}$, has an FOM of 0.79 at 300 keVee. Considering that its size remains
252 significantly large, this plastic is considered very efficient. Going forward, increasing the first dye
concentration, as in Sample #8, causes a FOM increase up to 0.88 at 300 keVee, as expected.
However, Sample #8 is smaller, $\text{Ø } 32 \text{ mm} \times \text{h } 27 \text{ mm}$, and the effect of the concentration increase on
PSD efficiency for our composition still needs to be assessed. Additionally, regarding PSD
deterioration of Sample #8 at energies above 500 keVee compared to Sample #6, this problem has
been solved in ongoing work and will be described elsewhere.

Regarding the concentration of the first fluorophore included, it seems that proportional to the volume
considered here, the FOM was not significantly increased. However, the study is ongoing and has
already yielded an efficient method of greatly optimizing PSD; this will be the subject of our next
publication.

258 *3.4. Comparison with literature data*

As an ultimate characterization of the PSD efficiency of our plastic scintillators, we have remade
260 plastic scintillators based on Zaitseva's preparation [6b] (see Table 1). Resulting samples #9 and 10,
without and with DPA as a secondary fluorophore, respectively, should be more or less equivalent to

262 industrial EJ-299-33 [12] in terms of PSD efficiency. Neutron/gamma discrimination spectra from
264 Samples #9 and 10 are presented in Figure 15.

INSERT FIGURE 15 HERE

266 Projections of bidimensional spectra of Samples #9 and 10 from Figure 15 at 400 keVee are presented
268 in Figure 16, where we can observe that their PSD efficiency appears equivalent.

INSERT FIGURE 16 HERE

272 Figures of Merit for Samples #9 and 10 are presented, and Table 5 provides a comparison with 3 other
274 plastics presented earlier (Samples #6 and 8 from our preparation at two different concentrations and
276 Sample #5, corresponding to the best of all Brooks' preparations but in which a modification has been
278 applied to the polymer matrix), allowing an ultimate comparison to be made. We observe that the
plastic we have developed, which is still under chemical optimization, already exhibits a PSD
efficiency comparable to those reported in the literature.

INSERT TABLE 5 HERE

280 In Figure 17, we compare Samples #5, 6, and 8 to Sample #9, which is based on the preparation
282 reported by Zaitseva *et al.*, which is considered the most efficient of its type. In addition, we have
284 included in Table 6 our data at $480 \text{ keVee} \pm 75 \text{ keVee}$ to compare to FOM from the EJ-299-33
industrial sample reported in Cester *et al.* [7].

INSERT FIGURE 17 HERE

INSERT TABLE 6 HERE

288 To add to Figure 17, we note that Zaitseva *et al.* [6b] characterized their sample under ^{252}Cf
290 irradiation, and that their preparation constitutes the basis of EJ-299-33 and the corresponding samples
292 that we have remade in our laboratory (Samples #9 and 10). Cester *et al.* [7] also characterized their
commercial sample under ^{252}Cf irradiation; however, in [6b] the source was shielded with 5.1 cm lead.
294 The sample from [6b] is $\text{Ø } 25 \text{ mm} \times \text{h } 25 \text{ mm}$, while that tested by Cester *et al.* is $\text{Ø } 50 \text{ mm} \times \text{h } 50$
mm and ours are $\text{Ø } 32 \text{ mm} \times \text{h } 16 \text{ mm}$.

296 Zaitseva *et al.* found FOMs of 2.82 and 3.31 at $480 \pm 75 \text{ keVee}$ (without and with DPA, respectively),
and while their preparation is comparable to our equivalent samples in terms of volume, energy and, in
our opinion, composition, we find FOMs of 1.01 and 1.06 at $480 \pm 75 \text{ keVee}$ for Sample #9 and 10.
298 However, the FOM calculation method most likely differs, and the shielding of the ^{252}Cf source
performed in [6b] may also cause the differences. The nature of the irradiating source, according to
300 some experiments we performed, should not affect FOMs in a significant manner. Additionally, when
compared to the FOM results reported by Cester *et al.*, in which a value of 1.29 was found at 480 ± 75
302 keVee, the volume is twice as large, which they propose as the source of the discrepancy. Again, in
this case [7], the source was unshielded.

304 If we compare all samples from Figure 17 only, Sample #9 (based on Zaitseva's formulation, PPO 30
wt% without 9,10-DPA) and Sample #8 (28.6 wt% of primary fluorophore with a small amount of

306 secondary fluorophore) display relatively stable FOMs on the whole energy spectrum when the same
307 volume is studied.

308 Comparing our recipe, Sample #6 (17 wt%), to the same volume of EJ-299-33 (Ø 50 mm × h 50 mm),
309 EJ-299-33's FOM reaches 1.29 , and Sample #6 0.90 both at 480 ± 75 keVee. Therefore, considering
310 statistical uncertainties, our preparation is 20 % lower in terms of PSD efficiency than EJ-299-33.
311 Higher FOM have been reached in ongoing work that will be presented elsewhere.

312

3.5. Light outputs

314 Sample #6 and 8, together with a BC-501A liquid scintillator and an EJ-200 plastic scintillator, have
315 been characterized in terms of Light Outputs (LO). LO for commercial samples are as follows:

- 316 - EJ-299-33: 8 600 ph/MeV at 1 MeVee [12],
- 317 - EJ-200: 10 000 ph/MeV at 1 MeVee (64% of anthracene) [13],
- 318 - BC-501A: 12 200 ph/MeV at 1 MeVee (78% of anthracene) [14].

319 LO are provided at 1 MeVee, relative to ^{22}Na CE located at 1.062 MeVee (see Table 2); this energy is
320 chosen to allow a comparison with data sheets from commercial scintillators. To obtain the number of
321 photons/MeV from the number of phe-/MeV, we divide by the PMT quantum efficiency (QE) as
322 described in Equation 3.

$$324 \quad \text{LO(ph/MeV)} = \left\{ \frac{\text{LO(phe-/MeV)}}{\text{PMT-QE}} \right\} \quad \text{Equation 4}$$

326 The QE for PMT XP-5500B is 39%, as described by Swiderski *et al.* [15]. The estimation of the QE is
327 usually provided with an error of approximately $\pm 10\%$ to which experimental uncertainty is added,
328 and LO was determined through 80% of the CEs at 1 MeVee. The results from our measurements are
329 comparable to values from the data sheets of BC-501A, EJ-200, and EJ-299-33 and are presented in
330 Table 7. They are comparable because we have tested BC-501A and EJ-200 in the same conditions,
331 then corrected our obtained values according to their data sheets at 1 MeVee. We were also able to
332 correct our results so as to be coherent in our overall comparison.

334 **INSERT TABLE 7 HERE**

336 Light Outputs observed for Samples #6 and 8 from our laboratory are modest in efficiency with values
337 half as good as EJ-299-33; however, improving the LO is part of the ongoing development process.

338 Count Rate measurements have been performed on a 17 wt% primary fluorophore + ϵ secondary
339 fluorophore plastic scintillator, along with a BC-408 [16] reference plastic scintillator of same size and
340 shape under the same set-up conditions. The results are provided in Table 8 as a percentage relative to
341 BC-408. The relative uncertainties in the results are approximately 10%. The Count Rate was almost
342 identical to the reference, except for ^{22}Na , where an unexplained discrepancy is observed.

344 **INSERT TABLE 8 HERE**

3.6. Market considerations

346 Potential industrial development of this new type of neutron/gamma discriminating scintillator
347 requires cheap scintillators. As the first fluorophore must be dissolved at a high concentration,
348 typically more than 10 wt%, its price must be as low as possible. For example, the preparation of a 10
349 $\times 10 \times 10$ cm³ cubic scintillator would require no less than 90 g of compound. Table 9 lists the prices

of the primary fluorophores used in this manuscript. It seems that our molecule would represent the lowest cost, being 30-fold cheaper than PPO. The most sophisticated fluorophores, 4-isopropylbiphenyl and 4-vinylbiphenyl, cannot compete with our molecule in terms of cost.

INSERT TABLE 9 HERE

Ultimately, we were able to produce a monolithic plastic scintillator with huge dimensions. As a proof of concept, a > 1 L sample (Ø 103 mm, length 114 mm) was prepared and did not exhibit any physical degradation after almost a year.

INSERT FIGURE 18 HERE

4. Conclusion

This work is divided into two closely related topics. First is the structure/activity relationship of various plastic scintillators which are able to perform a correct PSD between fast neutrons and gamma. In achieving this aim, the fluorophore must meet a number of criteria: absorb and emit light at approximately 300 nm and 360 nm, respectively, with the best possible photophysical parameters (fluorescence quantum yield, molar absorption coefficient, photobleaching), be highly soluble in non-polar media (such as styrene) and be stable to radiation. Among the > 50 formulations tested so far, we were able to produce a good composition of two different fluorophores, a primary and secondary, with the former being added at an optimum concentration of 28.6 wt%. As previously observed, a strong correlation was found between PSD capabilities (in terms of FOM) and the percentage of loading.

The potential stability issue was overcome by using cross-linked polymers instead of homopolymers of polystyrene or polyvinyltoluene. Thus, new plastic scintillators with good stability (> 3 years so far) have been obtained, with an FOM reaching 1.0 at 480 ± 75 keVee. A proof-of-concept, > 1 L large scintillator was prepared, showing that our technology is highly reliable, and this technology has the lowest price per gram (overall cost for chemicals < 1 €/g) compared to others on the market. Tested so far to the basic sensor level, PSD-capable plastic scintillators become both the most attractive and affordable technology. With medium-to-long term design integration suitable for portals, this could ultimately open the field to potential replacement of ^3He .

According to early results from Brooks and recent observations by Zaitseva, different mixtures of fluorophores in a polymer matrix can allow good and fast neutron/gamma discrimination, providing that a high loading of the first fluorophore is performed. This methodology can circumvent the low probability of two triplet states annihilating each other when they are stuck in infinitely viscous solutions. Moreover, our chemical composition is able to stabilize the material (the first samples were prepared in 2007) and enables the production of large plastic scintillators (> 1 L) with potentially good PSD and scintillation properties. Light outputs must still be increased. Additionally, many other points must be elucidated, and a complete theoretical understanding of neutron/gamma discrimination in plastic scintillators [10] will be truly appreciated.

Acknowledgments

Paweł Słobczyński and Joanna Iwanowska are acknowledged for their extensive help in recording Light Outputs. The Authors are indebted to Canberra for the grant provided to P. Blanc. This work was initiated with the support of the French governmental agency “Agence Nationale de la Recherche” and the NEUTROMANIA program.

References

- [1] F.D. Brooks, R.W. Pringle, B.L. Funt, IRE Trans. Nuc. Sci. NS-7 (1960) 35.
- [2] D.L. Horrocks, Rev. Sci. Instrum. 34 (1963) 1035.
- [3] (a) M. Hamel, V. Simic, S. Normand, React. Funct. Polym. 68 (2008) 1671; (b) R. Barillon, E. Bouajila, L. Douce, J.-M. Jung, L. Stuttgé, French Patent Application FR2933699, 2008; (c) N.L. Karavaeva, O.A. Tarasenko, Funct. Mater. 16 (2009) 92; (d) G. O'Bryan, A.L. Vance, S. Mrowka, N. Mascarenhas, Final LDRD Report, Sandia National Laboratories (2010); (e) M. Munier, PhD thesis, University of Strasbourg, 2012; (f) J. Iwanowska, L. Swiderski, M. Moszyński, T. Szczeńniak, P. Sibczyński, N.Z. Galunov, N.L. Karavaeva, JINST 6 (2011) P07007; (g) S. Carturan, A. Quaranta, T. Marchi, F. Gramegna, M. Degerlier, M. Cinausero, V.L. Kravchuk, M. Poggi, Rad. Prot. Dosimetry 143 (2011) 471; (h) M. Dalla Palma, A. Quaranta, T. Marchi, G. Collazuo, S. Carturan, F. Gramegna, M. Cinausero, IEEE proceedings of ANIMMA 2013, (2013).
- [4] M.A. Kovash, B. Daub, J. French, V. Henzl, K. Shoniyozov, J.L. Matthews, Z. Miller, H. Yang, IEEE proceedings of ANIMMA 2011 (2012).
- [5] (a) G. Corre, V. Kondrasovs, S. Normand, French Patent Application FR2947344, 2009; (b) S. Normand, V. Kondrasovs, G. Corre, J.-M. Bourbotte, A. Ferragut, IEEE proceedings of ANIMMA 2013, (2013); (c) R.R. Hansen, P.L. Reeder, A.J. Peurrung, D.C. Stromswold, IEEE Trans. Nuc. Sci. 47 (2000) 2024.
- [6] (a) N. Zaitseva, L. Carman, A. Glenn, S. Hamel, S.A. Payne, B.L. Rupert, PCT Patent Application 2012, WO2012142365; (b) N. Zaitseva, B.L. Rupert, I. Pawelczak, A. Glenn, H.P. Martinez, L. Carman, M. Faust, N. Cherepy, S. Payne, Nucl. Instr. and Meth. A 668 (2012) 88; (c) S. Nyibule, E. Henry, W.U. Schröder, J. Töke, L. Acosta, L. Auditore, G. Cardella, E. De Filippo, L. Francalanza, S. Giani, T. Minniti, E. Morgana, E.V. Pagano, S. Pirrone, G. Politi, L. Quattrocchi, F. Rizzo, P. Russotto, A. Trifirò, M. Trimarchi, Nucl. Instr. and Meth. A 728 (2013) 36; (d) S. Pozzi, M. Bourne, S. Clarke, Nucl. Instr. and Meth. A 723 (2013) 19. (e) A. Favalli, M.L. Iliev, K. Chung, C. Hurlbut, H.P. Martinez, M.T. Swinhoe, N.P. Zaitseva, K.D. Ianakiev, IEEE Trans. Nuc. Sci. 2013, 2.2, 1053-1056.
- [7] D. Cester, G. Nebbia, L. Stevanato, F. Pino, G. Viesti, Nucl. Instr. and Meth. A 735 (2014) 202.
- [8] P.L. Feng, J. Villone, K. Hattar, S. Mrowka, B.M. Wong, M.D. Allendorf, F.P. Doty, IEEE Trans. Nuc. Sci. 59 (2012) 3312.
- [9] M. Hamel, P. Blanc, C. Dehé-Pittance, S. Normand, French Patent Application 2013, FR1352072.
- [10] (a) P. Blanc, M. Hamel, L. Rocha, S. Normand, R. Pansu, IEEE Nuc. Sci. Symp. Conf. Rec. (2012) 1978; (b) M. Hamel, P. Blanc, L. Rocha, S. Normand, R. Pansu, Proc. SPIE 8710 (2013) 87101F.
- [11] C. Guerrero, D. Cano-Ott, M. Fernandez-Ordóñez, E. Gonzalez-Romero, T. Martinez, D. Villamarín, Nucl. Instr. and Meth. A 597 (2008) 212.
- [12] <http://www.eljentechnology.com/index.php/products/plastic-scintillators/114-ej-299-33> (last access February 17th, 2014).
- [13] <http://www.eljentechnology.com/index.php/products/plastic-scintillators/48-ej-200> (last access February 17th, 2014).
- [14] http://www.crystals.saint-gobain.com/uploadedFiles/SG-Crystals/Documents/SGC%20BC501_501A_519%20Data%20Sheet.pdf (last access February 17th, 2014).
- [15] L. Swiderski, M. Moszyński, D. Wolski, T. Batsch, A. Nassalski, A. Syntfeld-Każuch, T. Szczeńniak, F. Kniest, M. Kusner, G. Pausch, J. Stein, W. Klamra, IEEE Nuc. Sci. Symp. Conf. Rec. (2007) 1389.
- [16] <http://www.crystals.saint-gobain.com/Plastic-Scintillator.aspx> (last access February 17th, 2014).

Captions

Figure 1: Experimental set-up of the charge comparison method as PSD method for n/γ discrimination.

Figure 2: ^{22}Na and ^{137}Cs energy spectra from BC-501A liquid scintillator.

Figure 3: BC-501A neutron/gamma discrimination spectrum when exposed to an AmBe neutron source. Neutrons are located in the upper lobe of the graph, whereas gamma rays stand below. (The Y axis is $\times 10^3$).

Figure 4: Pictures of three scintillators where only the left one (a) succeeded in preparation process (Sample #1). All three are \varnothing 49 mm.

Scheme 1: Drawings of the chemicals.

Figure 5: Picture of Sample #3 after a month. Diameter is 30 mm.

Figure 6: Plastic Samples #1,2,4 and 5 respectively (a), (b), (c) and (d) neutron/gamma discrimination spectra when exposed to an AmBe neutron source. Neutrons are located in the upper lobe of the graph, whereas gamma rays stand below for each of the 4 samples presented. (The Y axis is $\times 10^3$).

Figure 7: Projection of BC-501A discrimination spectrum at 500 keVee \pm 10%.

Figure 8: Projections of Samples #1, 2, 4 and 5 discrimination spectra at 500 keVee \pm 10%.

Figure 9: Figures of Merit for Samples 1, 2, 4 and 5.

Figure 10: Neutron/gamma discrimination spectra from Samples #6 and 7 when exposed to an AmBe neutron source from the composition defined in our laboratory at 17 wt% of first fluorophore. (The Y axis is $\times 10^3$).

Figure 11: Neutron/gamma discrimination spectrum from Samples #8 when exposed to an AmBe neutron source from the composition defined in our laboratory at 28 wt% of first fluorophore. (The Y axis is $\times 10^3$).

Figure 12: Projections of Sample #6 and 7 discrimination spectra (both at 17 wt% concentration of first fluorophore) at 400 keVee \pm 10%.

Figure 13: Projection of Sample #8 discrimination spectra (at 28.6 wt% concentration of first fluorophore) at 400 keVee \pm 10%.

Figure 14: Figures of Merit from Samples #6, 7 and 8.

Figure 15: Neutron/gamma discrimination spectra from Samples #9 and 10 when exposed to an AmBe neutron source. (The Y axis is $\times 10^3$).

Figure 16: Projection of Samples #9 and 10 discrimination spectra (at 30 wt% concentration of PPO) at 400 keV \pm 10%.

Figure 17: Comparison of the Figures of Merit from 4 samples described in this paper under unshielded AmBe irradiation. Sample #9, most efficient of Zaitseva mixtures reproduced, Sample #6 and #7 two most efficient from our laboratory and Sample #5 most efficient from Brooks modified mixture.

Figure 18: Picture of Sample #11 with dimensions \varnothing 103 mm \times h 114 mm.

Figure 1
[Click here to download high resolution image](#)

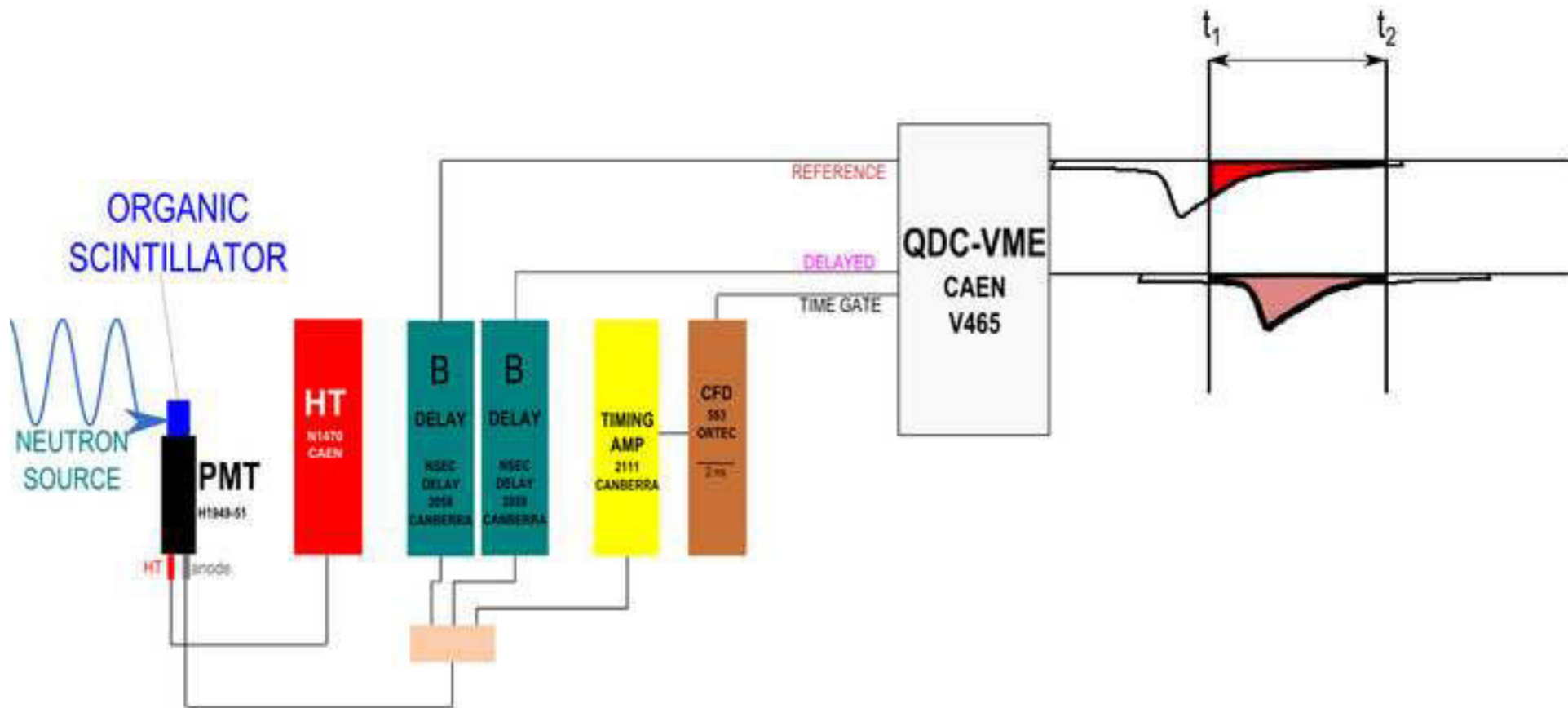


Figure 2
[Click here to download high resolution image](#)

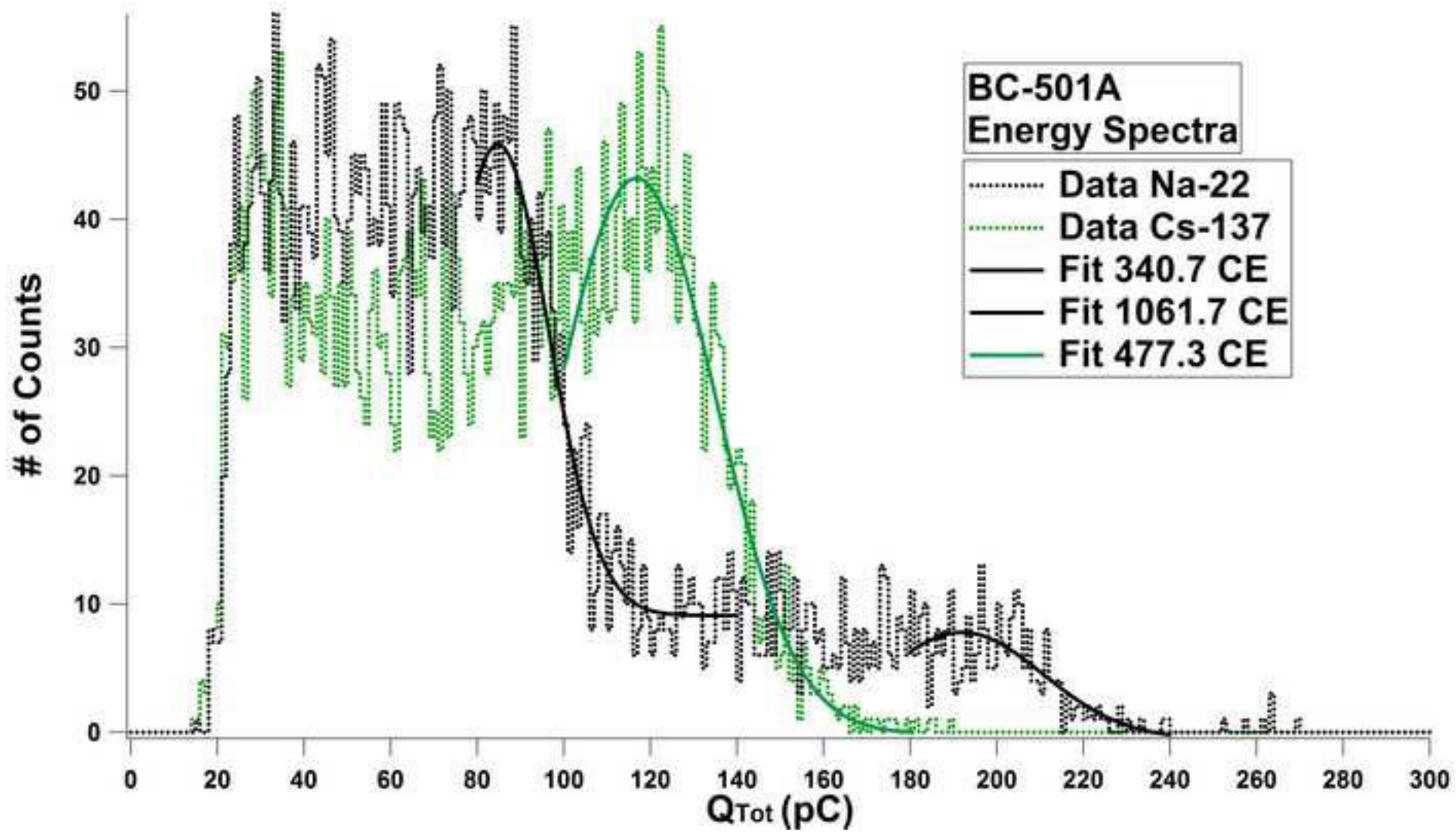


Figure 3
[Click here to download high resolution image](#)

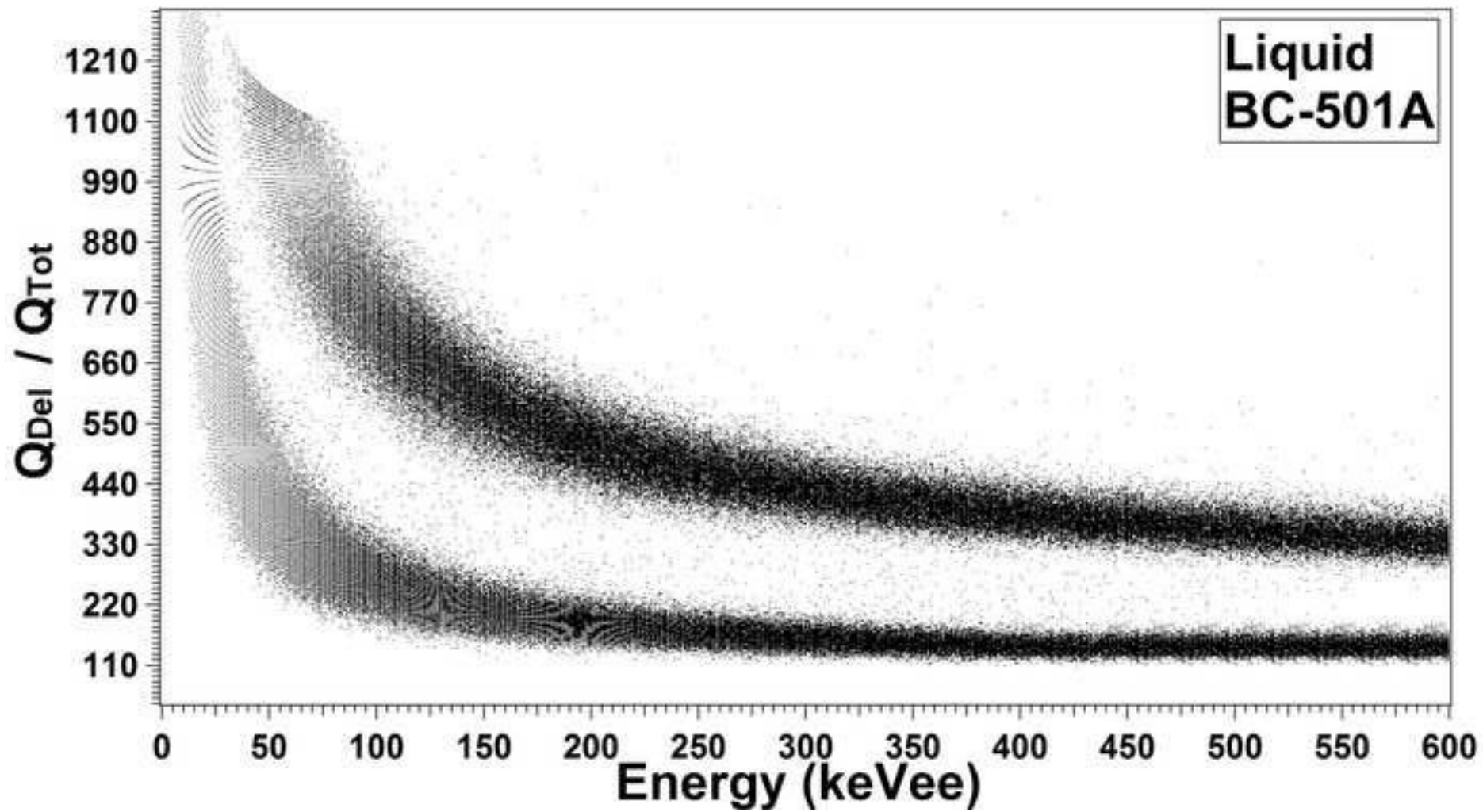


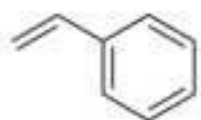
Figure 4
[Click here to download high resolution image](#)



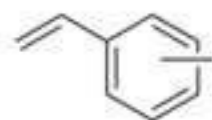
Scheme 1

[Click here to download high resolution image](#)

matrix:

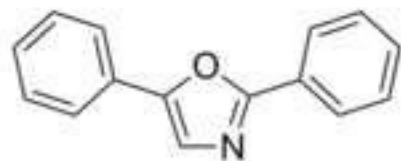


styrene



vinyltoluene

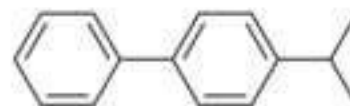
first fluorophore:



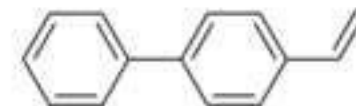
PPO



p-terphenyl

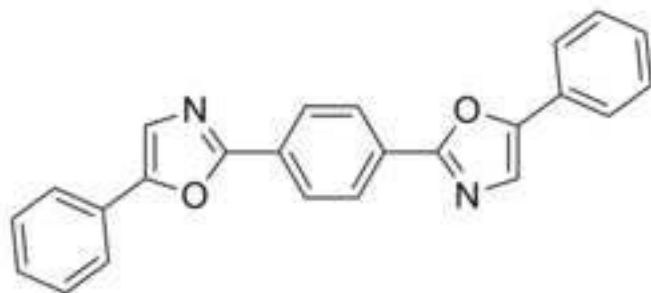


4-isopropylbiphenyl

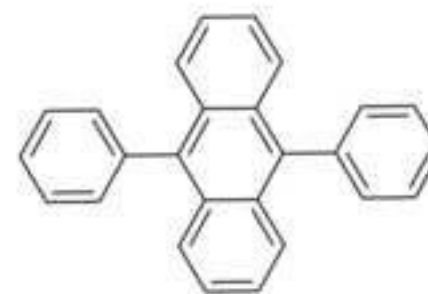


4-vinylbiphenyl

second fluorophore:



POPOP

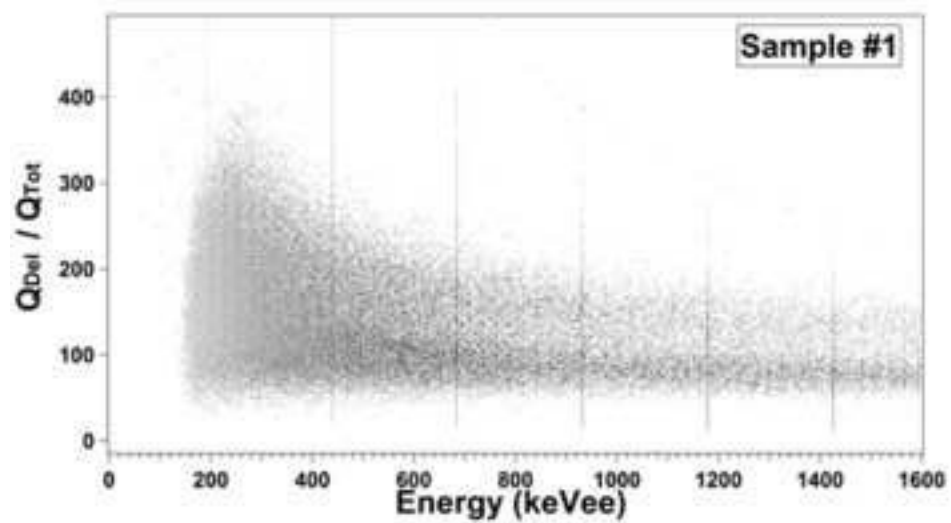


9,10-diphenylanthracene

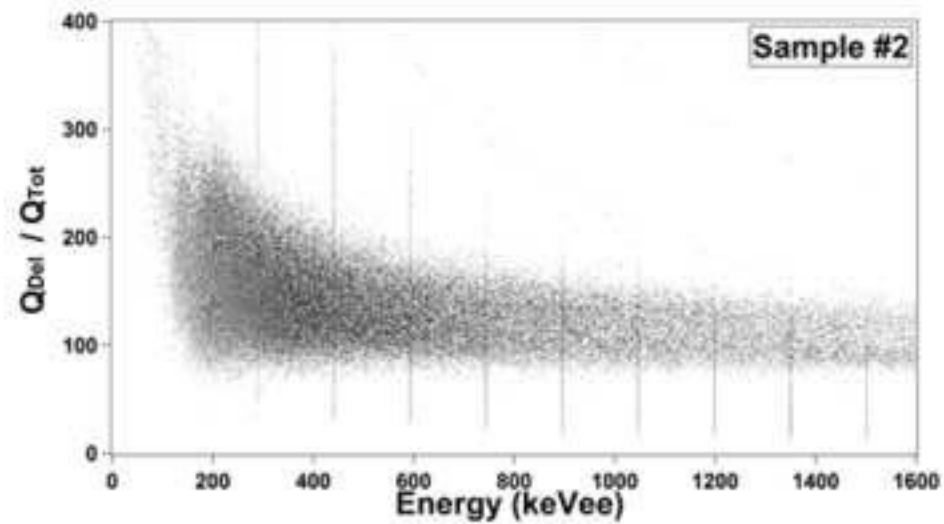
Figure 5
[Click here to download high resolution image](#)



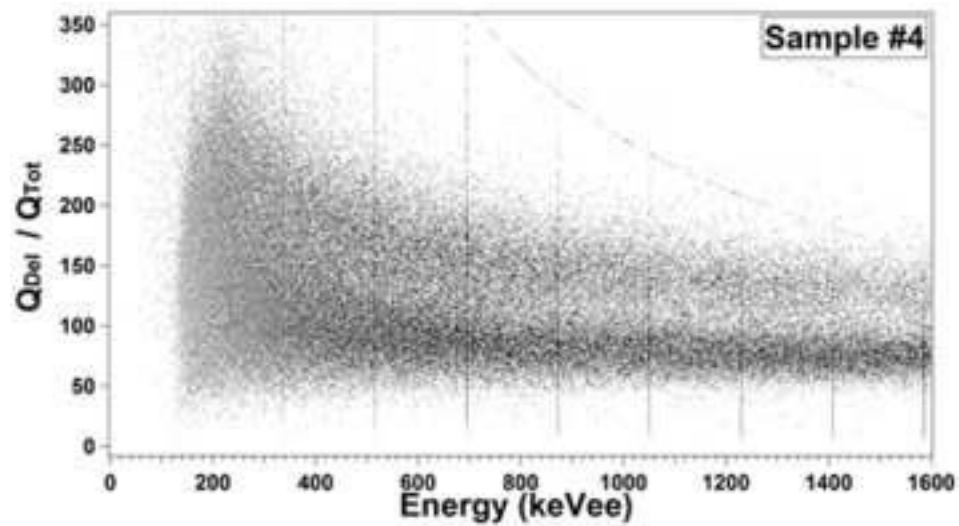
Figure 6
[Click here to download high resolution image](#)



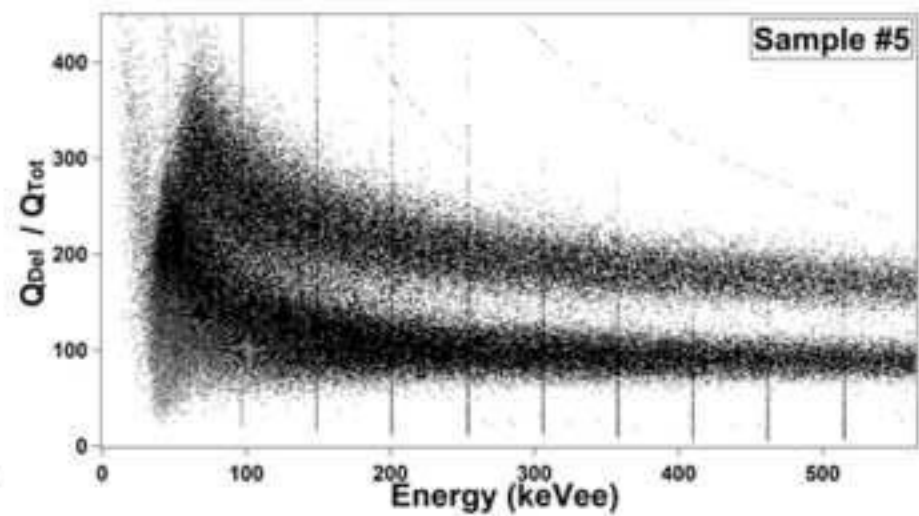
(a)



(b)



(c)



(d)

Figure 7
[Click here to download high resolution image](#)

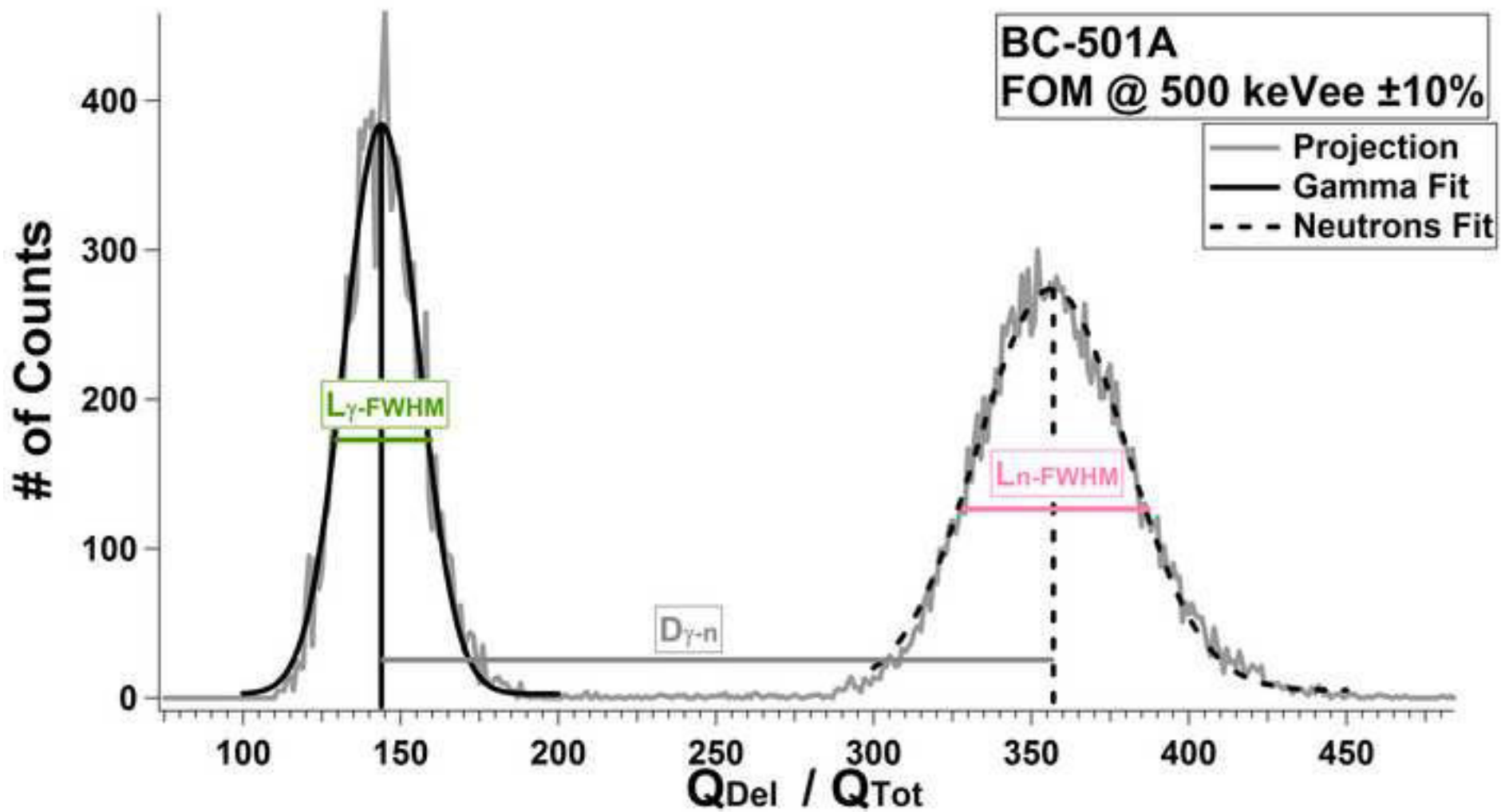
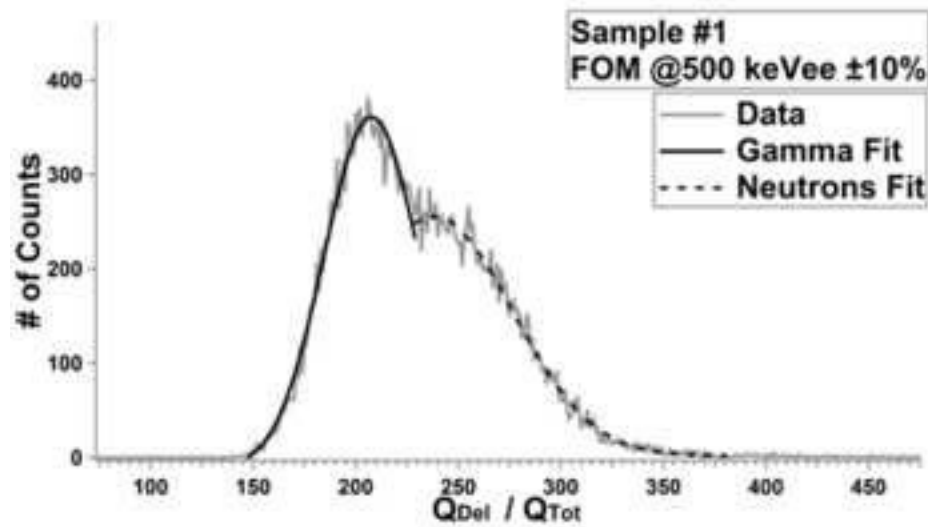
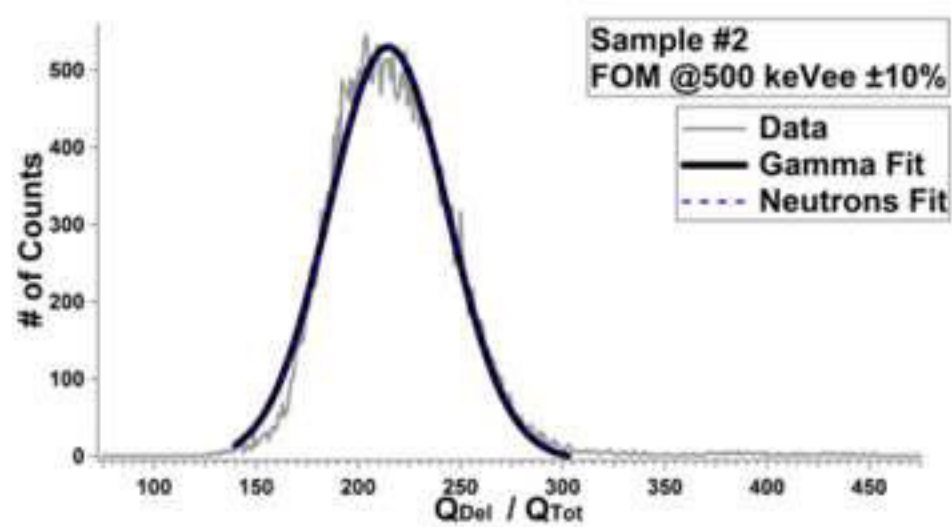


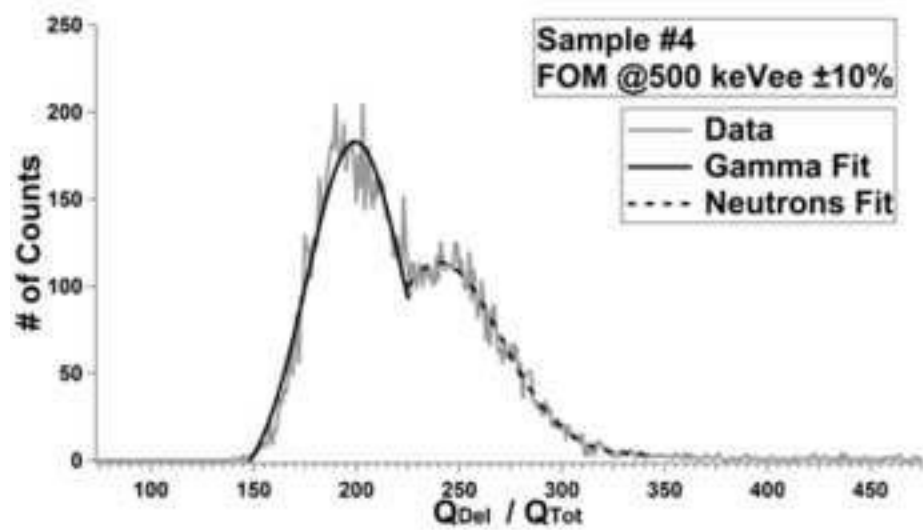
Figure 8
[Click here to download high resolution image](#)



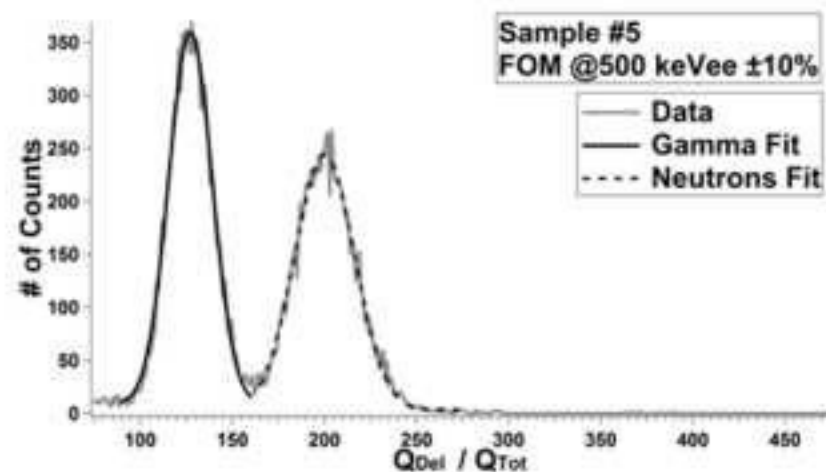
(a)



(b)



(c)



(d)

Figure 9
[Click here to download high resolution image](#)

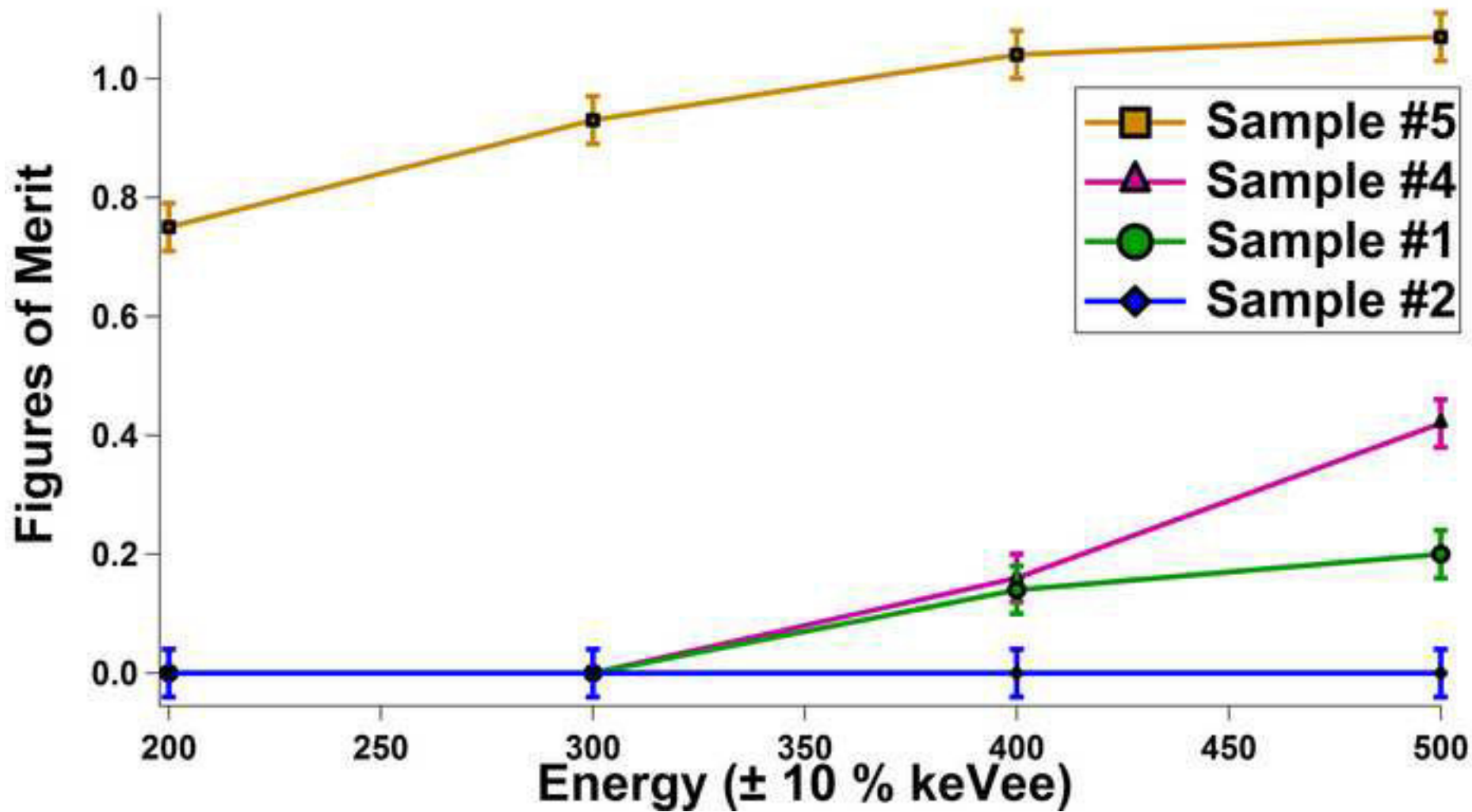
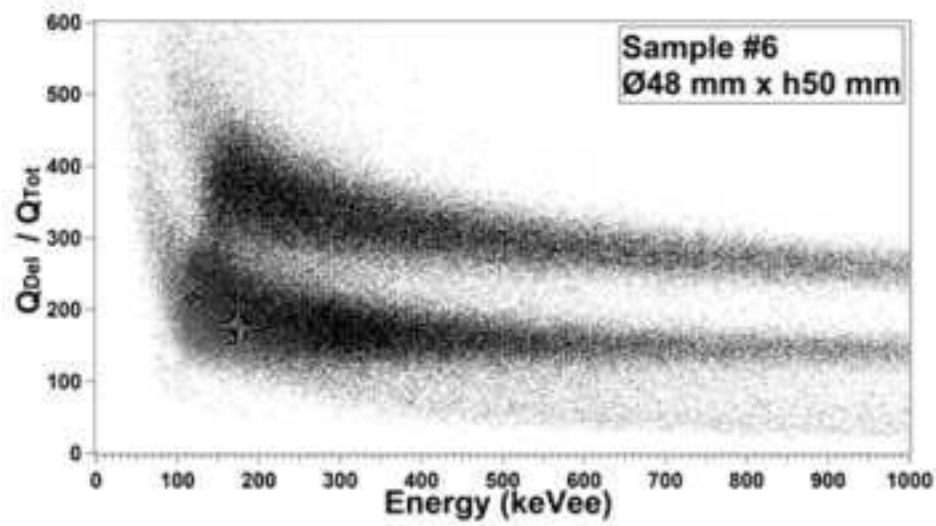
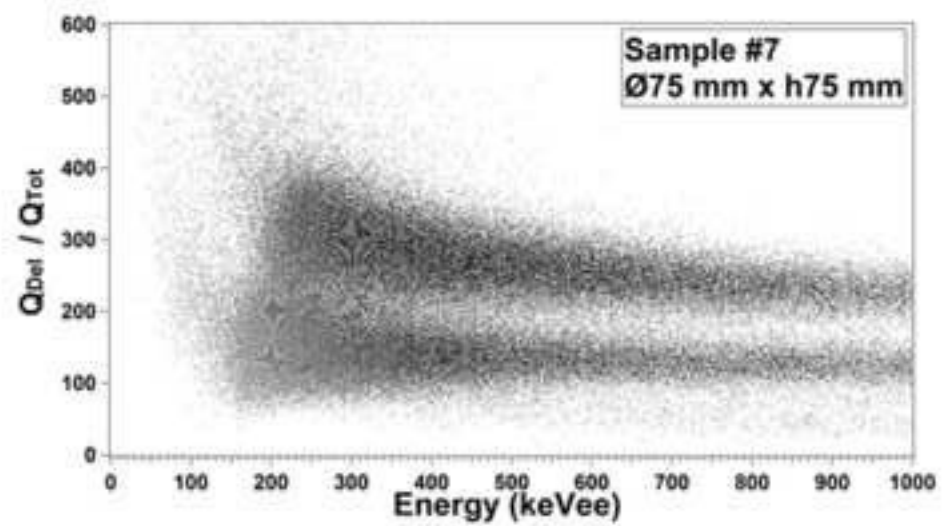


Figure 10
[Click here to download high resolution image](#)



(a)



(b)

Figure 11
[Click here to download high resolution image](#)

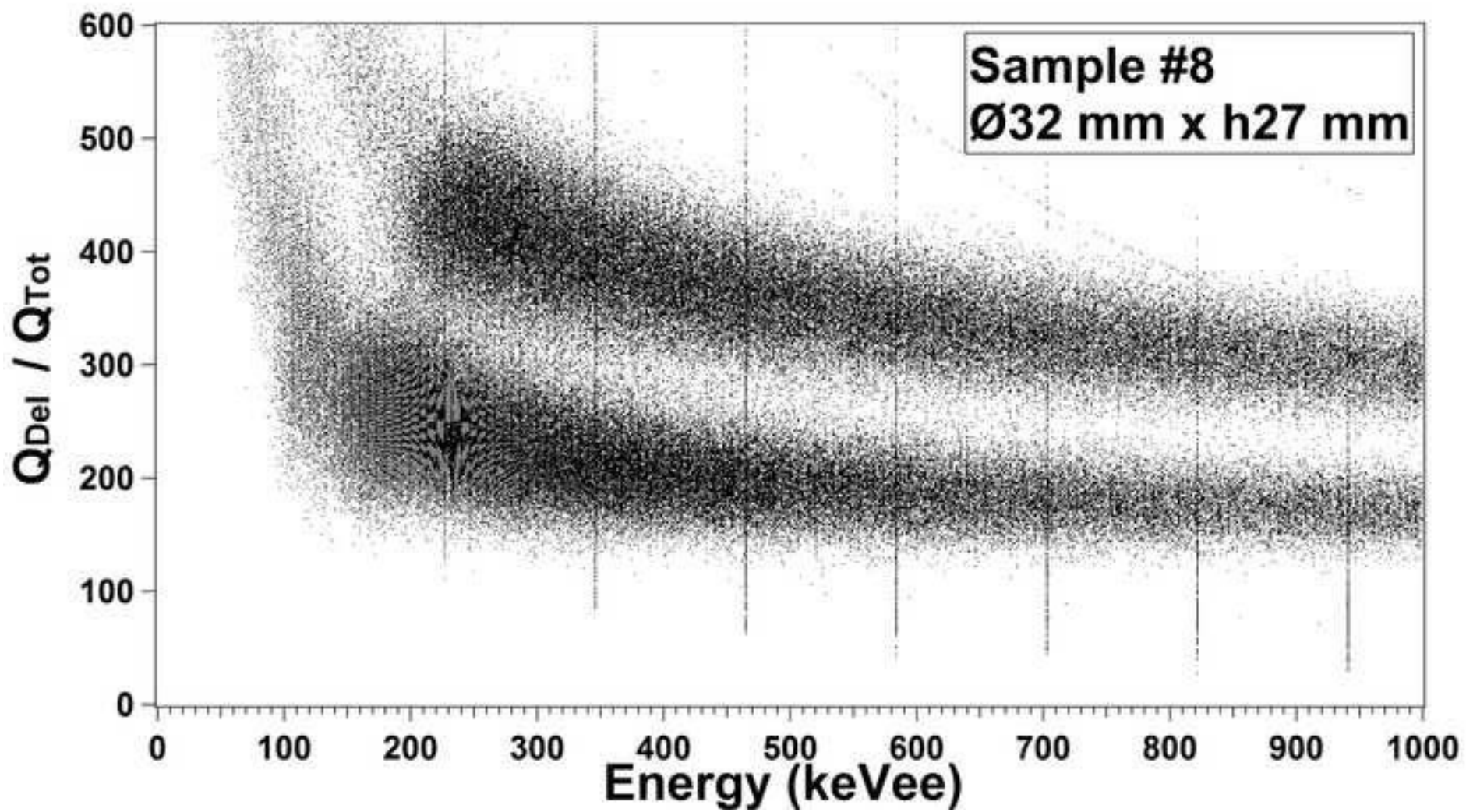
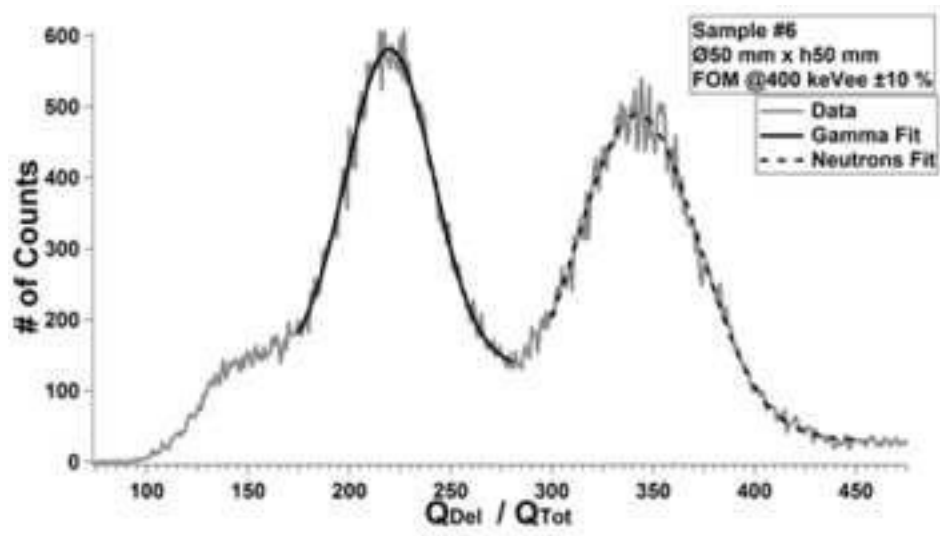
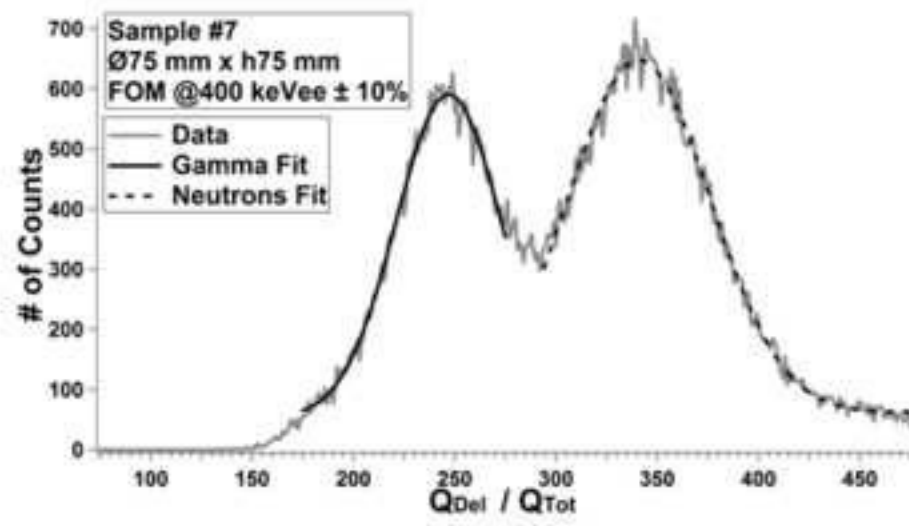


Figure 12
[Click here to download high resolution image](#)



(a)



(b)

Figure 13
[Click here to download high resolution image](#)

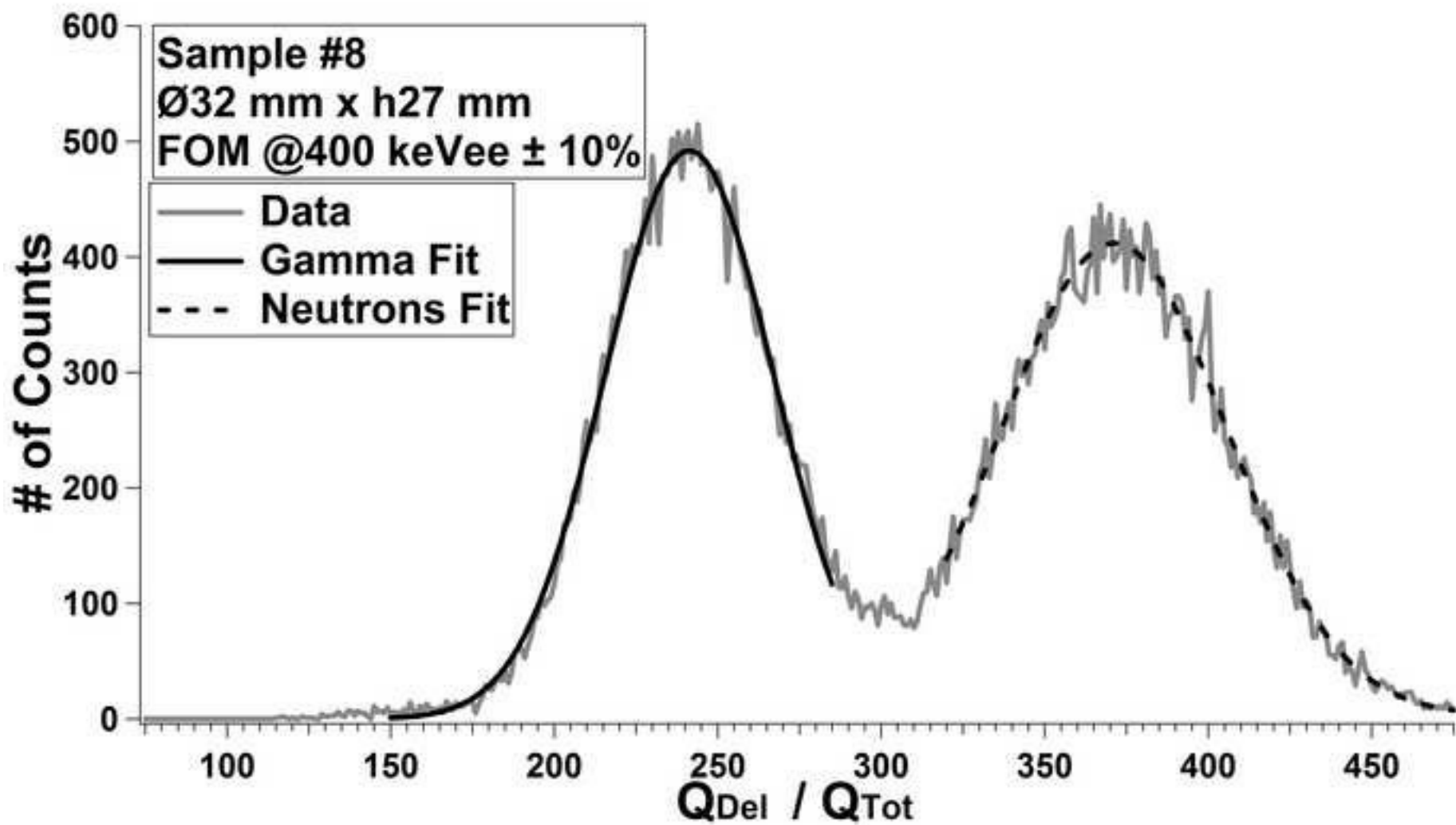


Figure 14
[Click here to download high resolution image](#)

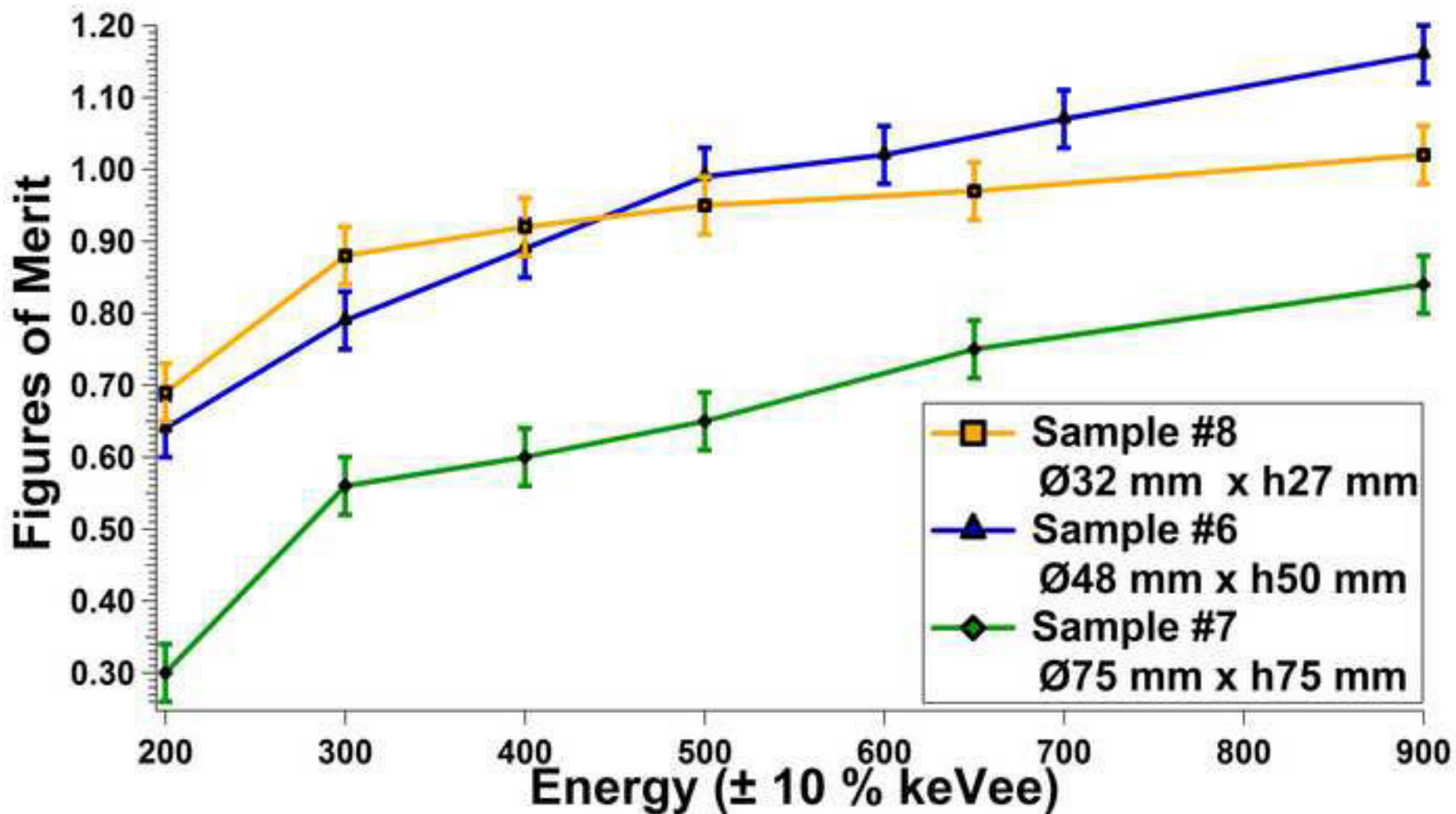
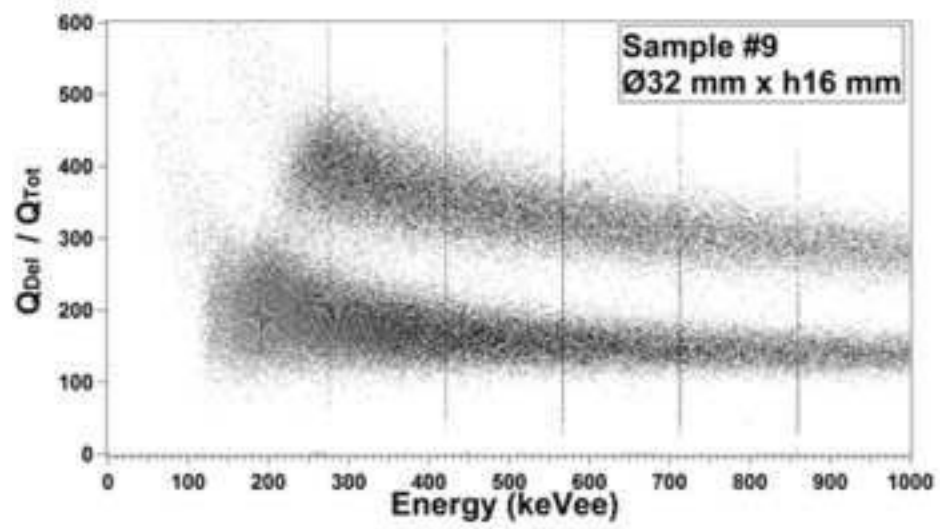
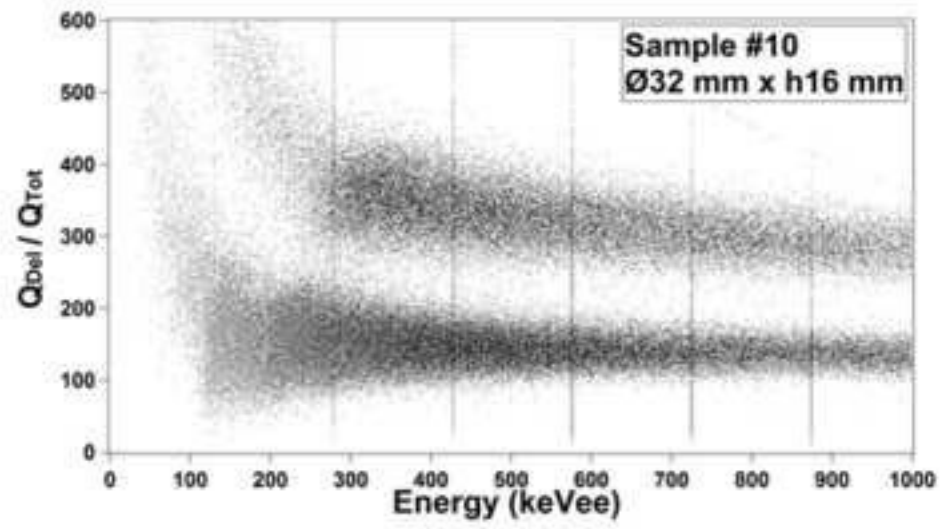


Figure 15
[Click here to download high resolution image](#)



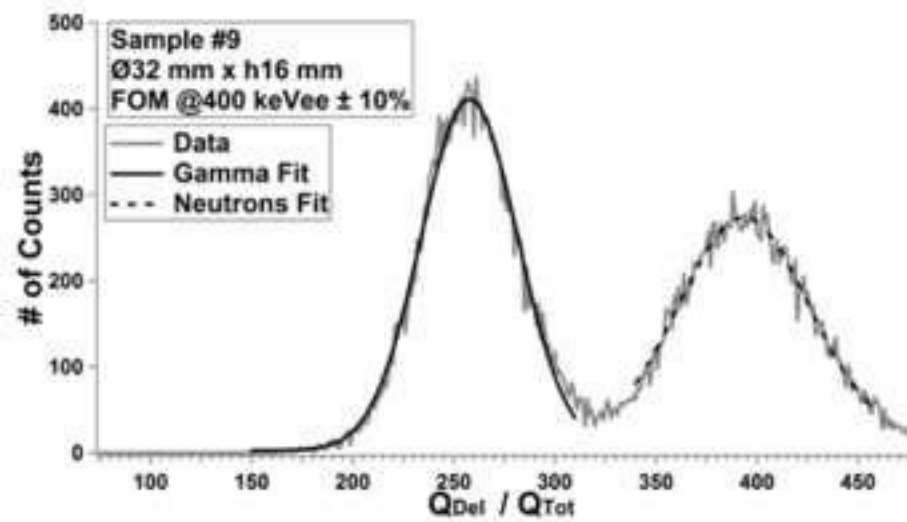
(a)



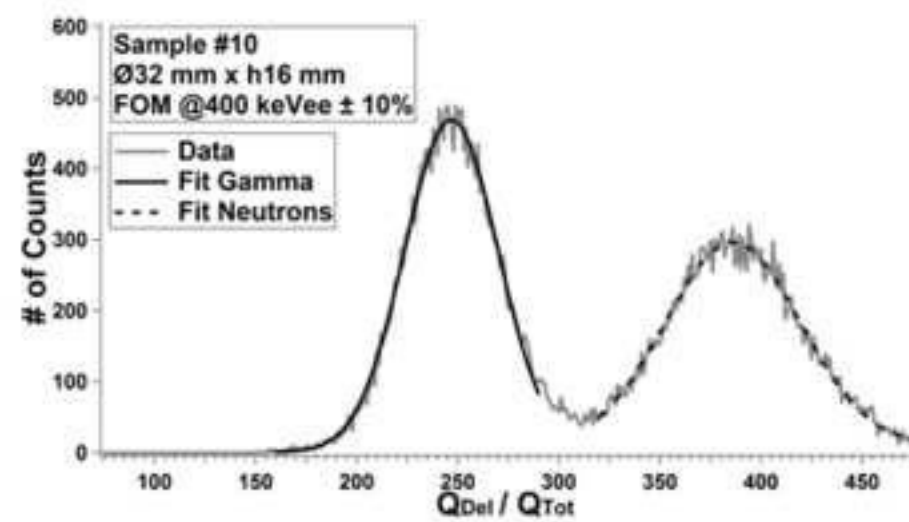
(b)

Figure 16

[Click here to download high resolution image](#)



(a)



(b)

Figure 17
[Click here to download high resolution image](#)

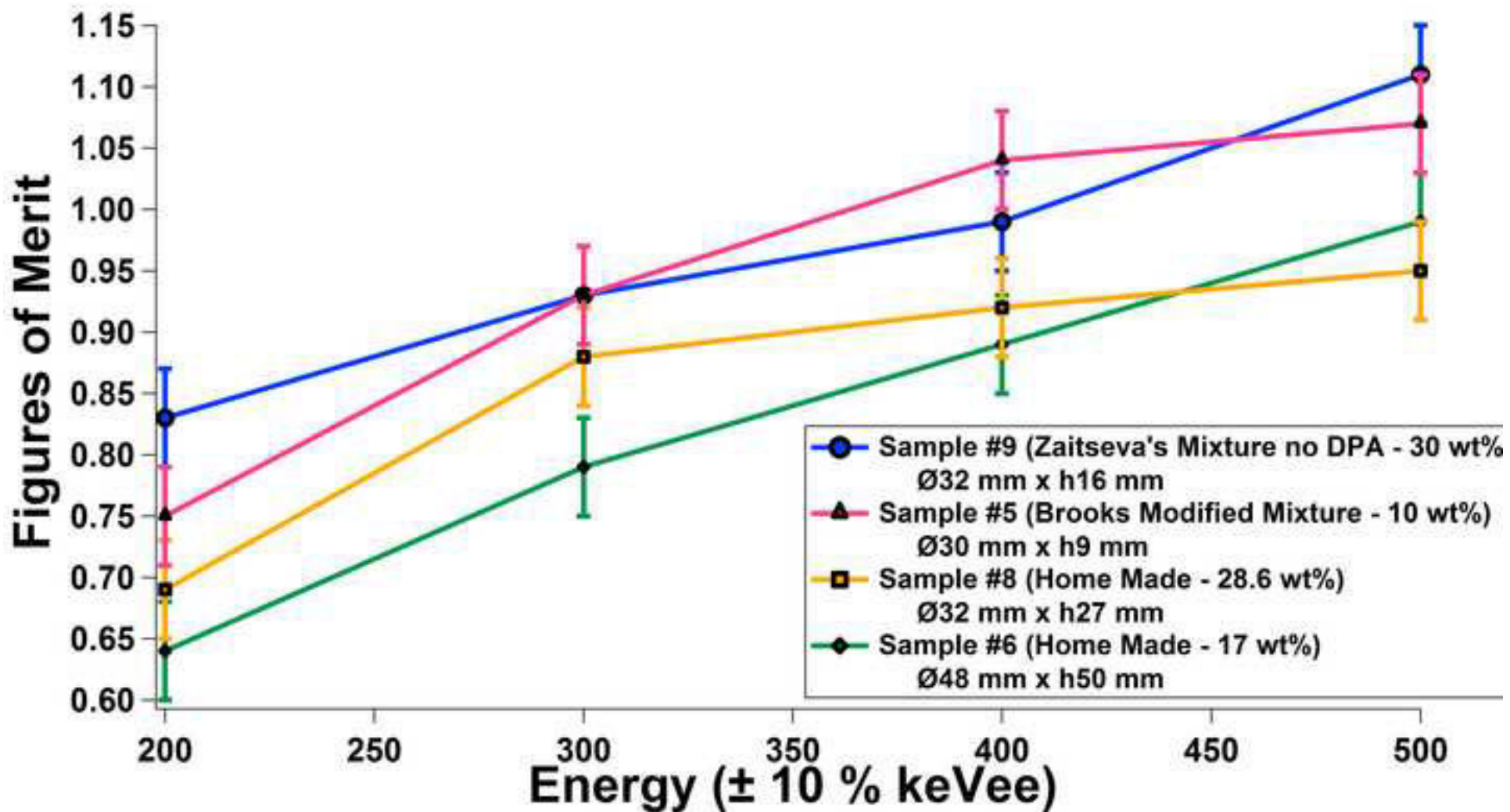


Figure 18
[Click here to download high resolution image](#)



Tables

Table 1: Main characteristics of the various plastic scintillators prepared.

Sample	Dimensions		1 st fluorophore (wt%)	2 nd fluorophore (wt%)	Observations
	Diameter (mm) Ø	Thickness (mm)			
#1	49	8	4-isopropylbiphenyl (10) and <i>p</i> -terphenyl (3.4)	POPOP (0.05)	From Plastic 77 Brook's recipe [1]
#2	30	13	4-isopropylbiphenyl (10)	POPOP (0.05)	Equiv. to #1 without <i>p</i> -terphenyl
#3	30	5	4-isopropylbiphenyl (15) and <i>p</i> -terphenyl (3.4)	POPOP (0.05)	4-isopropylbiphenyl more concentrated
#4	30	5	4-vinylbiphenyl (10)	POPOP (0.05)	Polymerizable fluorophore
#5	30	9	4-isopropylbiphenyl (10) and <i>p</i> -terphenyl (3.4)	POPOP (0.05)	Cross-linked polymer
#6	48	50	<i>Proprietary</i> (17)	Yes	Cross-linked polymer
#7	75	75	<i>Proprietary</i> (17)	Yes	Identical #6 but bigger
#8	32	27	<i>Proprietary</i> (29)	Yes	Cross-linked polymer
#9	32	16	PPO (30)	-	From Zaitseva's recipe [6]
#10	32	16	PPO (30)	DPA (0.2)	From Zaitseva's recipe [6]
#11	103	114	<i>Proprietary</i> (17)	Yes	Identical #6 & 7 but bigger

Table 2: Gamma energy and Compton edges of ²²Na and ¹³⁷Cs.

Gamma Sources	Gamma Energies E _γ (keV) #1	Gamma Energies (E _γ) (keV) #2	Compton Edges CE (keV) #1	Compton Edges CE (keV) #2
²² Na	511	1274.5	340.7	1061.7
¹³⁷ Cs	661.7		477.3	

Table 3: Figures of Merits from Brook's derivative samples compared to BC-501A from 200 to 500 keVee ±10%, σ ≈ ±0.05 for BC-501A and σ ≈ ±0.04 for all plastics.

Energy (keVee ± 10 %)	Liquid BC501-A	Sample #1	Sample #2	Sample #4	Sample #5
200	2.11	0.00	0.00	0.00	0.75
300	2.31	0.00	0.00	0.00	0.93
400	2.52	0.14	0.00	0.16	1.04
500	2.53	0.20	0.00	0.42	1.07

Table 4: Figures of Merits from Brooks' derivatives samples compared to BC-501A from 200 to 500 keVee ± 10%, σ ≈ ± 0.05 for BC-501A and σ ≈ ± 0.04 for all plastics.

Energy (keVee ± 10 %)	Liquid BC501-A	Sample #6	Sample #7	Sample #8
200	2.11	0.64	0.30	0.69
300	2.31	0.79	0.56	0.88
400	2.52	0.89	0.60	0.92
500	2.53	0.99	0.65	0.95

Table 5: Comparison of the Figures of Merit from 4 samples described in this paper. Sample #9, most efficient of Zaitseva mixture studied, Sample #6 and #8 two most efficient from our mixture, Sample #5 most efficient from Brook's modified mixture, σ ≈ ± 0.05 for BC-501A and σ ≈ ± 0.04 for all plastics.

Energy (keVee ±10%)	Liquid BC501-A	Sample #9	Sample #10	Sample #5	Sample #6	Sample #8
	Liquid Reference	Zaitseva's based mixture		Brook's based mixture	Lab Made mixture	
200	2.11	0.83	0.80	0.75	0.64	0.69
300	2.31	0.93	0.85	0.93	0.79	0.88
400	2.52	0.99	1.04	1.04	0.89	0.92
500	2.53	1.11	1.10	1.07	0.99	0.95

Table 6: Summary of FOM values at 480 keVee for EJ-299-33 efficiency comparison.

Energy	EJ-299-33	Sample #9	Sample #10	Sample #5	Sample #6	Sample #8
	Ref [7]	Zaitseva's based mixture		Brooks' based mixture	Lab Made mixture	
480 ± 75 keVee	1.29 ± 0.04	1.01 ± 0.04	1.06 ± 0.04	1.04 ± 0.04	0.90 ± 0.04	0.91 ± 0.04

Table 7: Light Output observed for different liquid and plastic scintillators.

Organic Scintillator	Observed LO (ph/MeV)	Corrected LO (Lit., ph/MeV)	Relative approximate Uncertainty
EJ-299-33 [12]	n.d.	8600	n.d.
EJ-200 [13]	6300	10 000	n.d.
BC-501A [14]	7300	12 200	n.d.
Sample #6	2100	3400	± 20 %
Sample #8	2100	3400	± 20 %

Table 8: Count Rates from 17 wt% loaded plastic scintillator normalized to reference BC-408.

Source	²² Na	¹³⁷ Cs	⁶⁰ Co	RSD
Count Rate (norm. BC-408)	65 %	90 %	95 %	± 10 %

Table 9: Prices per mmol for each primary fluorophore.

Fluorophore	CAS number	Molecular weight (g mol ⁻¹)	Provider	€ / mmol
4-isopropylbiphenyl	[7116-95-2]	196.29	Alfa Aesar	4.00
PPO	[92-71-7]	221.25	Acros or S-A	0.068
4-vinylbiphenyl	[2350-89-2]	180.25	Sigma-Aldrich	6.20
Proprietary fluorophore	-	-	-	0.002

Prices concern the product at the higher quantity available, with purity suitable for scintillation purpose, checked on August 29th, 2012, without any kind of discount. Considering the same matrix and the same secondary fluorophore, costs relative to them have been discarded.